Communication

Simulation of Fluid Flow During Direct Synthesis of H₂O₂ in a Microstructured Membrane Reactor

Laura L. Trinkies[1,*], Andrea Düll[1], Benedikt J. Deschner[1], Alexander Stroh[2], Manfred Kraut[1], and Roland Dittmeyer[1,3]

A microstructured membrane reactor has been developed to overcome the safety and productivity challenge of the direct synthesis of hydrogen peroxide. A single membrane is employed for separate, continuous dosage of the gaseous reactants hydrogen and oxygen to the solid catalyst present in the aqueous solvent. Using a custom OpenFOAM® model, the impact of catalyst-coated static mixers with different mixer geometries is studied. It is demonstrated that the custom fluid guiding elements outperform the investigated commercial static mixer under the flow conditions relevant to this application.

Keywords: Additive manufacturing, Flow chemistry, Hydrogen peroxide, Microreactor, Multiphase catalysis, OpenFOAM®

1 Introduction

Hydrogen peroxide (H₂O₂) is a promising "green" oxidant with application in paper, pulp and also wastewater treatment [1]. The most common production route for H₂O₂ today uses the anthraquinone auto-oxidation process [2], responsible for more than 95 % of the total H₂O₂ production [3]. With its high capital expenditures and required wastewater treatment [4], the process is currently only implemented at large scale, since it relies on the economy of scale to achieve viability [5]. An alternative reaction route is the direct synthesis of H₂O₂ by selective conversion of H₂ and O₂ over a solid catalyst [6,7]. Different combinations of active material, support and reaction medium for the direct synthesis of H₂O₂ exist, with an extended overview given in [5]. Nevertheless, all reaction systems studied for the direct synthesis route are facing the same safety concerns resulting from the direct contact of hydrogen and oxygen given the wide flammability range of the mixture [8,9].

One of the approaches to cope with this issue are membrane reactors [9,10]. They prevent direct hydrogen/oxygen contact by dosing one or both reactants through a membrane into an organic or inorganic solvent, which contains the solid catalyst [6, 10–12]. The major challenge in this kind of reactor is the development of a robust membrane [13]. Another concept to tackle the safety concerns are microreactors. Their narrow channels hinder the propagation of an explosion and therefore massively increase the range of safe operation [14]. The reactor concept presented in this paper combines both reactant separation with a membrane as well as microfluidic flow synergistically, targeting a new technology for on-site synthesis of ready-to-use hydrogen peroxide solutions [6,15].

In order to decrease the diffusion length at any fluid velocity contrary to suspension flow catalysis [6], we investigated catalytically coated inserts in the flow channels. Specifically, we used the design of so-called fluid guiding elements (FGEs), recently developed in our institute [16]. The impact of the inserts was investigated numerically in a CFD simulation using OpenFOAM® (OF) [17]. Special attention is given to the impact of the residence time and channel insert geometry on the reaction.

2 Materials and Methods

2.1 Design of the Membrane Reactor

Fig. 1a illustrates the reactor concept, which was adapted from an earlier reaction module designed in our institute [6]. The FGEs are produced using an additive manufacturing technology (laser-beam powder bed fusion, LB-PBF)

[1]Laura L. Trinkies, Andrea Düll, Benedikt J. Deschner, Manfred Kraut, Prof. Dr.-Ing. habil. Roland Dittmeyer
laura.trinkies@kit.edu
Karlsruhe Institute of Technology, Institute for Micro Process Engineering (IMVT), Hermann-von-Helmholtz-Platz, 76344 Eggenstein-Leopoldshafen, Germany.
[2]Dr.-Ing. Alexander Stroh
Karlsruhe Institute of Technology, Institute of Fluid Mechanics (ISTM), Kaiserstraße 10, 76131 Karlsruhe, Germany.
[3]Prof. Dr.-Ing. habil. Roland Dittmeyer
Karlsruhe Institute of Technology, Institute of Catalysis Research and Technology (IKFT), Hermann-von-Helmholtz-Platz 1, 76344 Eggenstein-Leopoldshafen, Germany.
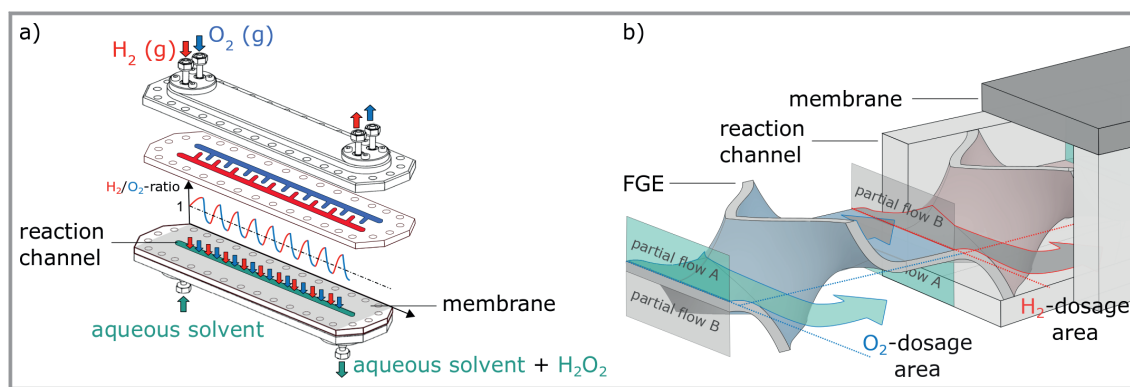
Figure 1. Sketch of the microstructured membrane reactor for the direct synthesis of H_2O_2 with gas resaturation, adapted with permission from Ref. [15] (a) and detailed scheme of the arrangement of a FGE in a microchannel covered by a PDMS membrane, adapted with permission from Ref. [34] (b).

which places some restrictions on the geometry, in particular avoiding overhangs [18]. For this reason, the curvilinear liquid channel design introduced by Selinsek et al. [6] was altered to a straight geometry while the gaseous reactants hydrogen and oxygen were introduced in an alternating manner over the dosing membrane, as illustrated in Fig. 1b. The FGEs do not generate turbulence but aim for a laminar guiding of the fluid flow to keep the pressure drop low by smart division and recombination of the flow and generated partial flows, respectively [16]. After partial flow A had contact with the mass transferring region for resaturation, the O_2- or H_2-dosage area in Fig. 1b, it is directly guided away from the place of exchange to the channel bottom to equilibrate. Then, the next equilibrated partial flow B is led to the region of transfer. The contact time of the fluid with the gas was kept short to keep the diffusion depth of the resaturating gas considerably small in order to guarantee a large concentration gradient and thereby enhance the mass transfer. The same principle has previously been described for heat transfer.

2.2 Material Properties

The transport and material properties are summarized in Tab. 1, with all properties corresponding to a temperature of 298 K (simulations were run at this temperature, and future experiments will be conducted at this temperature). The influence of the additives H_2SO_4 and NaBr on the fluid properties of the aqueous reaction medium were neglected. Similarly, due to the low solute concentrations expected, it was

assumed that the dissolved species H_2, O_2 and H_2O_2 did not alter the fluid properties. Only binary diffusion of the individual solutes in the liquid reaction medium as described by the Fickian diffusion model was considered. The simple solution diffusion model, as described in [19], was used to model the mass transport through the dense polymer membrane.

A 5-wt % Pd/TiO$_2$ catalyst was chosen as model catalyst for this study applied as a coating onto the microstructured channel inserts. This palladium loading is among the highest reported for defined nanocatalysts [24] and was therefore selected for an enhanced but realistic reactor productivity. Since the kinetics are yet to be determined in a purely aqueous reaction medium containing $0.15 \, \text{mol m}^{-3}$ H_2SO_4 and $4 \, \text{mol m}^{-3}$ NaBr, the numerical simulation adapted the kinetic model from Voloshin et al. [25–28] for a system with close resemblance to the specific combination of catalyst and reaction medium present. The adapted kinetic rate expressions considered in the numerical simulation are presented in Eqs. (1) and (5) with the adapted constants given in Eqs. (2)–(4) and (6)–(8) [25–28].

$$r_{\text{hydrogenation}} = \frac{k_h^\star c_{H_2} c_{H_2O_2}}{\left[1 + \left(K_{H_2,h}^\star c_{H_2}\right)^{1/2} + \left(K_{H_2O_2,h}^\star c_{H_2O_2}\right)^{1/2}\right]^4} \quad (1)$$

with

$$k_h{}^\star = \frac{k_h K_{H_2,h} K_{H_2O_2,h}}{H_{H_2}} \quad (2)$$

Table 1. Transport and material properties at 298 K.

Property	H_2	O_2	H_2O_2	H_2O	Reference
D_{i,H_2O} [m²s⁻¹]	$3.894 \cdot 10^{-9}$	$2.488 \cdot 10^{-9}$	$2.298 \cdot 10^{-9}$	–	[20]
ν_{H_2O} [m²s⁻¹]	–	–	–	$8.927 \cdot 10^{-7}$	[21]
H_i [mol m⁻³Pa⁻¹]	$7.800 \cdot 10^{-6}$	$12.000 \cdot 10^{-6}$	–	–	[22]
P_i [mol m⁻²s⁻¹Pa⁻¹]	$1.77 \cdot 10^{-7}$	$1.12 \cdot 10^{-7}$	0	0	[23]

$$K_{H_2,h}{}^\star = \frac{K_{H_2,h}}{H_{H_2}} \tag{3}$$

$$K_{H_2O_2,h}{}^\star = K_{H_2O_2,h} \tag{4}$$

$$r_{\text{formation, }H_2O_2} = \frac{k_f^\star c_{H_2} c_{O_2}}{\left[1 + K_{H_2,f}^\star c_{H_2} + K_{O_2,f}^\star c_{O_2}\right]^2} \tag{5}$$

with

$$k_f{}^\star = \frac{k_f K_{H_2,f} K_{O_2,f}}{H_{H_2} H_{O_2}} \tag{6}$$

$$K_{H_2,f}{}^\star = \frac{K_{H_2,f}}{H_{H_2}} \tag{7}$$

$$K_{O_2,f}{}^\star = \frac{K_{O_2,f}}{H_{O_2}} \tag{8}$$

Moreover, a layer thickness of 4 μm with a porosity ε of 0.4 and tortuosity τ of 6, reported for silica coatings employed in the direct synthesis was assumed for all simulated structures [29]. Although Gemo et al. [30] provided the experimental proof of negligible internal mass transfer limitations within a comparable operation range for a spherical catalyst of 15 μm diameter, the impact of mass transfer limitations within the catalyst coating layer on the macroscopic reaction rates of the direct synthesis of H_2O_2 was considered by effectiveness factors. This allowed further studies of a wider catalyst layer range. The effectiveness factors were calculated using Matlab®. All kinetic parameters used are listed in Tab. 2 and 3.

Table 2. Kinetic constants of the proposed rate expressions: pre-exponential factors k_0 and sorption equilibrium constants K_i at system temperature according to [25, 27]; subscripts: h for the hydrogenation reaction path and f for the H_2O_2 formation reaction path.

Property	Value
$k_{0,h}$ [mol$_{H2O2}$kg$_{cat}^{-1}$s^{-1}]	$25.57 \cdot 10^6$
$K_{0,H2,h}$ [Pa^{-1}]	$3.36 \cdot 10^{-10}$
$K_{0,H2O2,h}$ [m^{3}mol^{-1}]	$2.95 \cdot 10^{-4}$
$k_{0,f}$ [mol$_{H2O2}$kg$_{cat}^{-1}$s^{-1}]	$1.60 \cdot 10^3$
$K_{0,H2,f}$ [Pa^{-1}]	$2.76 \cdot 10^{-4}$
$K_{0,O2,f}$ [Pa^{-1}]	$3.38 \cdot 10^{-8}$

2.3 Numerical Model of the Reactor

OF provides a finite-volume-based framework for the creation of custom computational solvers for continuum mechanics problems [17]. The CAD model of the FGEs generated in Autodesk® Inventor® was used via STL format import to create the numerical grid using OF meshing tools. The simulation domain consisted of a rectangular channel,

Table 3. Kinetic constants of the proposed rate expressions: activation energy E_a and reaction enthalpy ΔH_i according to [25, 27]; subscripts: h for the hydrogenation reaction path and f for the H_2O_2 formation reaction path.

Property	Value
$E_{a,h}$ [kJ mol^{-1}]	43.7
$\Delta H_{H2,h}$ [kJ mol^{-1}]	−23.1
$\Delta H_{H2O2,h}$ [kJ mol^{-1}]	−4.7
$E_{a,f}$ [kJ mol^{-1}]	22.3
$\Delta H_{H2,f}$ [kJ mol^{-1}]	10.1
$\Delta H_{H2O2,f}$ [kJ mol^{-1}]	−12.2

which contained the microstructured FGE inserts. The channel used for the investigations had a width of 6 mm, a height of 1.97 mm and a length of 44.5 mm. Additional inlet and outlet zones of 11 mm length each were implemented in order to guarantee a fully developed flow. These zones equal the maximum expected hydrodynamic entrance length calculated analytically.

In the simulation, the flow regime present in the liquid channel was assumed to be laminar, due to the low liquid flow rates in the range of milliliters per minute as used in the concept presented in [6] and [15] as well as channel geometries in the millimeter range. The maximum expected Reynolds number Re calculated in a void rectangular channel with a width of 6 mm and a height of 1.97 mm for an estimated, elevated flow rate of 16 mL min^{-1} was 75, which confirmed the validity of this assumption. Moreover, the system was considered isothermal and the flow field incompressible due to the nature of the aqueous reaction medium under the conditions given.

Three phases are present in the actual reactor, namely the gaseous H_2 and O_2 flowing through separate reactor channels, the solid membrane and the solid catalyst applied onto microstructured FGEs as well as the liquid reaction medium. To simplify the problem, a single-phase model was adopted for the simulation by merely considering the liquid phase with the dissolved reactants and the product. Thus, the membrane and the catalyst coating were defined as system boundaries. Moreover, it was assumed that the feeding gas phases remain constant in their composition, even in case of possible cross-contamination of the H_2-gas channel with O_2 by desaturating gas and vice versa. This is justified in case of the gas channels being flushed sufficiently and permanently with the corresponding pure gas. Fig. 2 shows a schematic representation of the simulated geometry. The implemented patches of the simulation and the applied boundary conditions can be taken from Fig. 3.

OF's *blockMesh* utility was used for the background mesh, while *snappyHexMesh* was used to generate the computational grid so that the FGE features were captured correctly and high gradient regions were resolved particularly well. Mass diffusion processes impose much stricter constraints
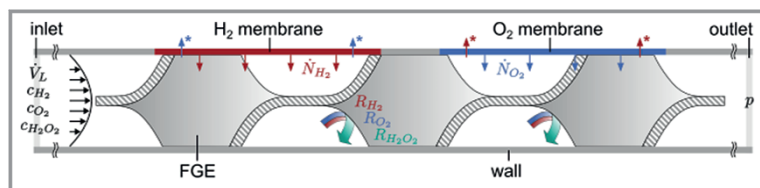
Figure 2. Schematic representation of the simulated geometry, showing the boundaries, fixed quantities and species flows across the system boundaries; transmembrane flows causing H_2/O_2 cross-contamination indicated with an asterisk (*).

$$\frac{\partial}{\partial t}\left(\vec{v}\right) + \nabla \cdot \left(\vec{v}\,\vec{v}\right) = -\frac{1}{\rho}\nabla p + \nu\nabla^2\vec{v} \tag{11}$$

To solve the species conservation equation (Eq. (12)) for the concentration, *PBiCGStab* with diagonal-based incomplete LU preconditioner (*DILU*) was used.

$$\nabla \cdot \left(c_i\,\vec{v}\right) - \nabla \cdot (D_i\nabla c_i) = 0 \tag{12}$$

on mesh resolution than fluid dynamics [31]. Thus, at least three cell layers were used within the concentration boundary layer to ensure the proper capture of concentration gradients and mass transport phenomena as recommended by Bothe and Reusken [31]. Correspondingly, three additional grid layers were added within a distance of 0.03 mm, which is lower than the expected minimum concentration boundary layer thickness estimated from mass transfer correlations. To ensure sufficient grid refinement, different grid resolutions were investigated and their maximum residuals as well as the resulting maximum species imbalances were evaluated as control quantities. The acceptable residual for a stable result was set to $1 \cdot 10^{-4}$ for the concentration. The errors obtained from mass and individual species balances applied to the overall system had to be below the threshold of 1 %. A grid of 7 million cells of an average size of 10^{-13} m^{-3} was finally used in the simulation.

To evaluate the velocity, the iterative solver *smoothSolver* with symmetric Gauss-Seidel smoother (*symGaussSeidel*) was used in OF to solve the conservation of mass equation (Eq. (9)) for an incompressible fluid with the nabla operator ∇ (Eq. (10)).

$$\frac{\partial}{\partial t}\rho + \nabla \cdot \left(\rho\vec{v}\right) = 0 \tag{9}$$

$$\nabla \cdot \vec{v} = 0 \tag{10}$$

For the pressure, on the other hand, the iterative solver *GAMG* with Gauss-Seidel smoother (*GaussSeidel*) was employed to solve the momentum conservation equation (Eq. (11)) under the assumption of incompressible flow, constant dynamic viscosity μ and absence of volume forces.

In order to include the description of the catalyst-coated FGEs, a Neumann boundary condition *catWall* derived from the OF class *fixedGradientFvPatchFields* was implemented. During the evaluation of the species conservation equation, the *catWall* boundary face concentrations were then determined from the corresponding values at the cell centroid and the previously calculated effective reaction rates as formulated in Eq. (13) and (14)

$$c_{i,bf} = c_{i,c} + \delta_{bf-c}\left(\frac{R_i^A}{D_i}\right) \tag{13}$$

with

$$R_i^A = r_i\big(c_{H_2}, c_{O2}, c_{H_2O_2}\big)\eta_i\big(c_{H_2}, c_{O_2}, c_{H_2O_2}\big)\rho_{wc}\delta_{wc}. \tag{14}$$

At every face belonging to a *membraneWall* patch, the boundary face value $c_{i,bf}$ was calculated from the cell value in dependence of the species's partial pressure in the gas phase $p_{i,G}$, the membrane permeance P_i, properties such as the Henry constant H_i and diffusion coefficient D_i as well as the cell's face-to-center distance δ_{bf-c} according to Eq. (15).

$$c_{i,bf} = \frac{\frac{P_i}{H_i}}{\frac{D_i}{\delta_{bf-c}}+\frac{P_i}{H_i}}p_{i,G}H_i + \frac{\frac{D_i}{\delta_{bf-c}}}{\frac{D_i}{\delta_{bf-c}}+\frac{P_i}{H_i}}c_{i,c} \tag{15}$$

The derived solver was verified by the comparison with the (semi-)analytical solutions of three different configurations of a simplified, cylindrical channel geometry evaluated using Matlab®.
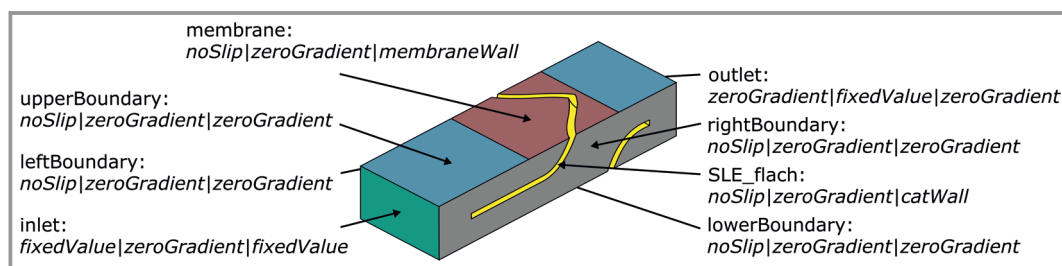

Figure 3. Boundary conditions applied to *velocity (U)* | *pressure (p)* | *concentration (c)* fields at the different patches.

www.cit-journal.com

© 2021 The Authors. Chemie Ingenieur Technik published by Wiley-VCH GmbH

Chem. Ing. Tech. **2021**, *93*, No. 5, 1–8

2.4 Considered Case: Influence of the Geometry of the Microstructured Channel Insert on Reactor Performance

As the catalyst is applied as a coating onto the microstructured channel inserts, the inserted structure's geometry is expected to have a considerable influence on the reactor performance. This was investigated by carrying out CFD simulations with two different geometries of mixing inserts. A commercial static mixer (SMX®, from Sulzer AG, Winterthur, Switzerland) with a geometry adapted from [32] was compared with a customized FGE developed in our institute. While the inserts' overall widths, heights and lengths are identical, the surface area of SMX® available for the application of catalyst exceeds the FGE's surface area with an area ratio S_{SMX}/S_{FGE} of 2.27. Similarly, the volume reduction of the liquid flow channel due to the inserted structure was higher in case of the SMX® resulting from its slightly bigger volume. This leads to a volume ratio of the resulting liquid volumes of $V_{L,SMX}/V_{L,FGE} = 0.94$. The influence of the volumetric flow rate was evaluated by carrying out simulations with both geometries over range between 0.7 and 15.9 mL min⁻¹. The system pressure and temperature were set to 2 bar and 298 K. In all simulations, a membrane arrangement of alternating H_2 and O_2 dosing zones of 2 mm length each and a distance of 1.27 mm in between was chosen.

3 Results and Discussion

A comparison of the pressure drop over the length of the liquid flow channel for the case of no insert, the SMX®
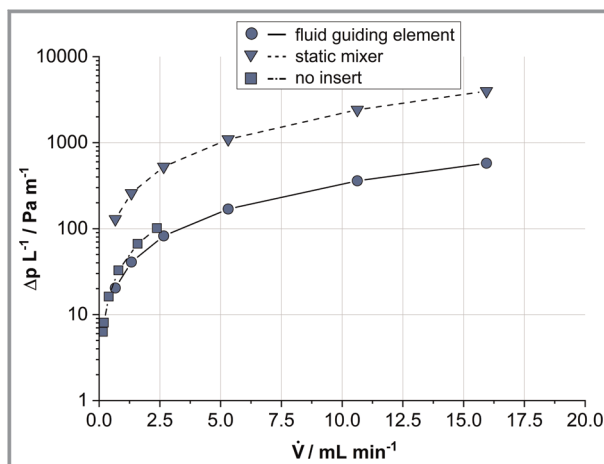

Figure 4. Pressure drop Δp over the length of the reactor as a function of the volumetric flow rate $\dot{V}$ with the 45 mm long SMX® and FGE serving as channel inserts at 2 bar and volume flows between 0.7 and 15.9 mL min⁻¹.

insert and FGE insert is shown in Fig. 4. At low residence times (corresponding to higher flow velocities) the pressure drop for SMX® inserts is significantly higher than for FGE inserts. At higher residence times, the difference between the pressure drop for SMX® versus FGE is smaller. The calculated H_2O_2 outlet concentrations $c_{H2O2,out}$ achieved with the two different types of microstructured channel inserts are compared in Fig. 5a. Fig. 5b shows the comparison of the H_2O_2 outlet concentrations $c_{H2O2,out}$ per surface area of the respective insert S_{insert}. As a reference, the corresponding values for a void channel without inserts but with catalyst coated lower and side walls are given additionally in all graphs.
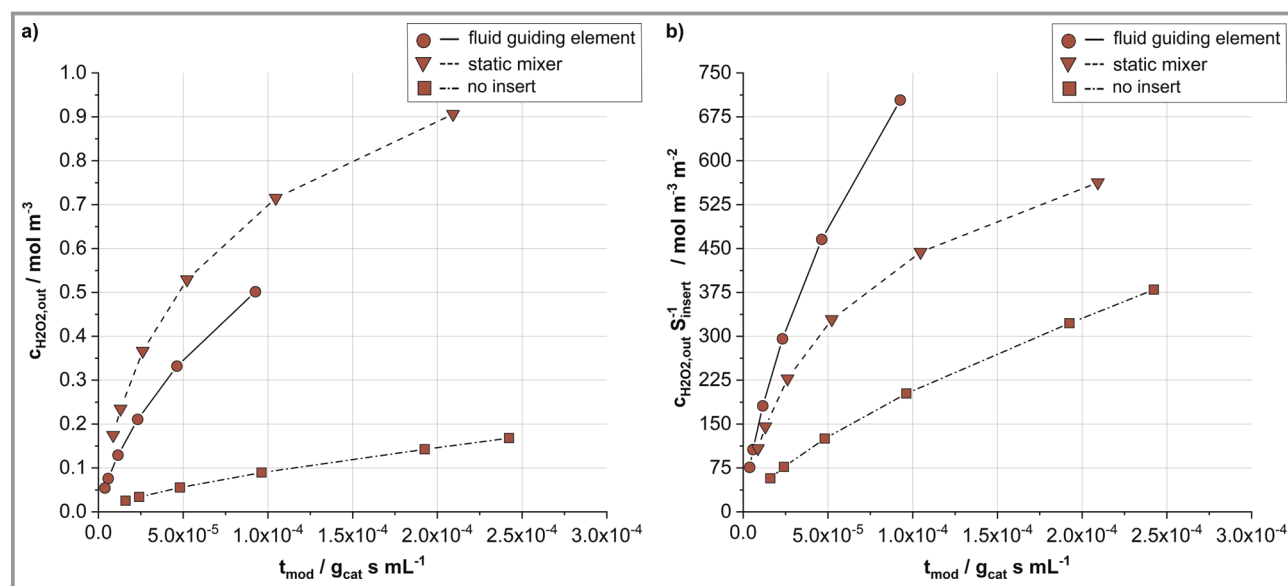

Figure 5. Average product outlet concentration $c_{H2O2,out}$ in dependence of the modified residence time t_{mod}. 45 mm long SMX® and FGE serving as channel inserts at 2 bar and volume flows between 0.7 and 15.9 mL min⁻¹ (a). Influence of the geometry of the microstructured channel insert's geometry on the achieved $c_{H2O2,out}$ relative to the insert's surface area S_{insert} under the same flow conditions (b).

At all investigated modified residence times ($m_{cat}/\dot{V}$), the performance of the reactor with SMX® inserts in terms of $c_{H2O2,out}$ appears to be superior to the one with FGE inserts (Fig. 5a). This is to be attributed to the SMX's higher surface area and the corresponding increased amount of catalyst present in the system, the H_2O_2 outlet concentration ratio $c_{H2O2,SMX}/c_{H2O2,FGE}$ exceeds the surface area ratio S_{SMX}/S_{FGE} at all residence times. This may be explained by an enhancement of the SMX's mixing properties at increased liquid velocities in the laminar flow regime, which is consistent with findings of Rahmani et al. [33]. On the other hand, the FGE is beneficial in terms of the overall pressure drop (Fig. 4) over the length of the liquid flow channel as the structure does not contain any abrupt changes in its geometry and thus imposes less resistance to the liquid flow [16]. It can also be seen from Fig. 5b that the achieved H_2O_2 outlet concentration relative to the insert's surface area of the FGE (i.e., the productivity per catalyst mass) is even significantly higher than the one of the SMX® at all residence times. With H_2O_2 hydrogenation as consecutive reaction path in the reaction network, comparably low residence times (high t_{mod}) proved to be beneficial [15], which is why it may be concluded that the implementation of catalyst-coated FGEs has a beneficial effect on the reaction system.

4 Conclusion

In the simulations presented, the influence of the microstructured insert's geometry on the reactor performance quantified by the H_2O_2-outlet concentration $c_{H2O2,out}$ was investigated at different volumetric flow rates by comparing a FGE insert with a standard SMX® at different flow rates. Higher product concentrations in general were found to be achieved with the latter. This is attributed to the static mixer's higher surface area and therefore high amount of catalyst present in the system. The use of FGEs, however, is beneficial in terms of pressure drop at lower residence times and higher productivity relative to a defined catalyst mass is achieved.

To conclude, the basis has been laid for the optimization of a microstructured membrane microreactor for the direct synthesis of H_2O_2 facilitated by spatially resolved CFD simulations. Further research will validate the implemented solver against experimental results, paving the way to a precise reaction control of this demanding multiphase reaction.

Symbols used

$D_{i,H2O}$	[m^{2}s^{-1}]	Fickian diffusion coefficient of gas i in H_2O
c	[mol m^{-3}]	molar concentration
$c_{i,bf}$	[mol m^{-3}]	concentration of the gas i at the boundary face
$c_{i,inlet}$	[mol m^{-3}]	concentration of the gas i at the inlet of the simulated field
$c_{i,sat}$	[mol m^{-3}]	saturation concentration of the gas i, according to Henry's law
H_i	[mol m^{-3}Pa^{-1}]	Henry constant of gas i
ΔH_i	[J mol^{-1}]	reaction enthalpy
K	[Pa^{-1}]	sorption equilibrium constant
k	[–]	kinetic rate constant
k_0	[–]	pre-exponential factor (reaction rate)
L	[m]	length
m_{cat}	[g]	catalyst mass
p_i	[Pa]	partial pressure of gas i
R_i	[–]	rate of generation or destruction of species i due to chemical reactions
r	[mol s^{-1}kg^{-1}]	reaction rate per catalyst mass
T	[K]	temperature
t_{mod}	[g$_{coat}$s mL^{-1}]	modified residence time
$S_{SMX/FGE}$	[m^2]	surface area of the inserts (SMX®/FGE)
S_{insert}	[m^2]	surface area of the respective insert
v	[m s^{-1}]	velocity
$V_{L,SMX/FGE}$	[m^{-3}]	volume in the liquid channel after implementing the insert (SMX®/FGE)
$\dot{V}$	[mL min^{-1}]	volumetric flow rate

Greek letters

δ	[m]	distance, thickness
ε	[–]	porosity
η	[–]	catalyst effectiveness factor
μ	[Pa s]	dynamic viscosity
ν_{H2O}	[m^{2}s^{-1}]	kinematic viscosity of H_2O
τ	[–]	tortuosity
ρ	[kg m^{-3}]	material density
P_i	[mol m^{-2}s^{-1}Pa^{-1}]	membrane permeance of gas i

Sub- and Superscripts

A	per unit area
bf	boundary face
c	center
G	gas
H_2	hydrogen

H$_2$O$_2$	hydrogen peroxide
L	liquid
O$_2$	oxygen
wc	wallcoat
*	adapted property
$\vec{x}$	vector quantity x

Abbreviations

FGE	fluid guiding element
PDMS	polydimethylsiloxane
PET	polyethylene terephthalate
PI	polyimide
OF	OpenFoam®

References

[1] G. Goor, J. Glenneberg, S. Jacobi, J. Dadabhoy, E. Candido, in *Ullmann's Encyclopedia of Industrial Chemistry*, Wiley-VCH Verlag, Weinheim **2000**.

[2] N. M. Wilson, D. T. Bregante, P. Priyadarshini, D. W. Flaherty, in *Catalysis* (Eds: J. Spivey, Y.-F. Han), Royal Society of Chemistry, Cambridge **2017**, 112–212.

[3] Y. Yi, L. Wang, G. Li, H. Guo, *Catal. Sci. Technol.* **2016**, *6 (6)*, 1593–1610. DOI: https://doi.org/10.1039/C5CY01567G

[4] N. Gemo, T. Salmi, P. Biasi, *React. Chem. Eng.* **2016**, *1 (3)*, 300–312. DOI: https://doi.org/10.1039/C5RE00073D

[5] C. Samanta, *Appl. Catal. A* **2008**, *350 (2)*, 133–149. DOI: https://doi.org/10.1016/j.apcata.2008.07.043

[6] M. Selinsek, M. Bohrer, B. K. Vankayala, K. Haas-Santo, M. Kraut, R. Dittmeyer, *Catal. Today* **2016**, *268*, 85–94. DOI: https://doi.org/10.1016/j.cattod.2016.02.003

[7] H. Henkel, W. Weber, *Patent US1108752A*, **1913**.

[8] G. Centi, S. Perathoner, S. Abate, in *Modern heterogeneous oxidation catalysis* (Ed: N. Mizuno), Wiley-VCH, Weinheim **2009**.

[9] J. García-Serna, T. Moreno, P. Biasi, M. J. Cocero, J.-P. Mikkola, T. O. Salmi, *Green Chem.* **2014**, *16 (5)*, 2320. DOI: https://doi.org/10.1039/c3gc41600c

[10] A. Pashkova, R. Dittmeyer, N. Kaltenborn, H. Richter, *Chem. Eng. J.* **2010**, *165 (3)*, 924–933. DOI: https://doi.org/10.1016/j.cej.2010.10.011

[11] A. Pashkova, K. Svajda, R. Dittmeyer, *Chem. Eng. J.* **2008**, *139 (1)*, 165–171. DOI: https://doi.org/10.1016/j.cej.2007.09.003

[12] A. Pashkova, L. Greiner, U. Krtschil, C. Hofmann, R. Zapf, *Appl. Catal. A* **2013**, *464–465*, 281–287. DOI: https://doi.org/10.1016/j.apcata.2013.06.007

[13] S. Abate, S. Melada, G. Centi, S. Perathoner, F. Pinna, G. Stukul, *Catal. Today* **2006**, *117 (1–3)*, 193–198. DOI: https://doi.org/10.1016/j.cattod.2006.05.050

[14] C. Liebner, H. Hieronymus, S. Heinrich, F. Edeling, T. Lange, E. Klemm, in *Beiträge zum 13. BAM-PTB-Kolloquium zur chemischen und physikalischen Sicherheitstechnik am 18. und 19. Juni 2013 in Braunschweig* (Eds: M. Beyer, T. Stolz), Fachverlag NW in Carl Schünemann Verl. GmbH, Bremen **2014**.

[15] M. Selinsek, M. Kraut, R. Dittmeyer, *Catalysts* **2018**, *8 (11)*, 556. DOI: https://doi.org/10.3390/catal8110556

[16] E. Hansjosten, A. Wenka, A. Hensel, W. Benzinger, M. Klumpp, R. Dittmeyer, *Chem. Eng. Process.* **2018**, *130 (May)*, 119–126. DOI: https://doi.org/10.1016/j.cep.2018.05.022

[17] H. G. Weller, G. Tabor, H. Jasak, C. Fureby, *Comput. Phys.* **1998**, *12 (6)*, 620. DOI: https://doi.org/10.1063/1.168744

[18] J.-P. Kruth, B. Vandenbroucke, J. Vaerenbergh, P. Mercelis, *International Conference Polymers & Moulds Innovations (PMI)*, Gent, Belgium, April **2005**.

[19] *Membranverfahren: Grundlagen der Modul- und Anlagenauslegung* (Eds: T. Melin, R. Rautenbach), 2nd ed., Springer, Berlin **2004**.

[20] M. Selinsek, A. Pashkova, R. Dittmeyer, *Catal. Today* **2015**, *248*, 101–107. DOI: https://doi.org/10.1016/j.cattod.2014.05.048

[21] *VDI-Wärmeatlas*, 11th ed., Springer Vieweg, Berlin **2013**.

[22] R. Sander, *Atmos. Chem. Phys.* **2015**, *15 (8)*, 4399–4981. DOI: https://doi.org/10.5194/acp-15-4399-2015

[23] M.-B. Hägg, *J. Membr. Sci.* **2000**, *170 (2)*, 173–190. DOI: https://doi.org/10.1016/S0376-7388(99)00371-3

[24] S. Wang, D. E. Doronkin, M. Hähsler, X. Huang, D. Wang, J.-D. Grunwaldt, S. Behrens, *ChemSusChem* **2020**, *13 (12)*, 3243–3251. DOI: https://doi.org/10.1002/cssc.202000407

[25] Y. Voloshin, R. Halder, A. Lawal, *Catal. Today* **2007**, *125 (1–2)*, 40–47. DOI: https://doi.org/10.1016/j.cattod.2007.01.043

[26] Y. Voloshin, J. Manganaro, A. Lawal, *Ind. Eng. Chem. Res.* **2008**, *47 (21)*, 8119–8125. DOI: https://doi.org/10.1021/ie8000452

[27] Y. Voloshin, A. Lawal, *Appl. Catal. A* **2009**, *353 (1)*, 9–16. DOI: https://doi.org/10.1016/j.apcata.2008.10.019

[28] Y. Voloshin, A. Lawal, *Chem. Eng. Sci.* **2010**, *65 (2)*, 1028–1036. DOI: https://doi.org/10.1016/j.ces.2009.09.056

[29] V. Paunovic, *Direct synthesis of hydrogen peroxide in a wall-coated capillary microreactor*, Ph. D. Thesis, Technische Universität Eindhoven **2015**.

[30] N. Gemo, P. Biasi, P. Canu, T. O. Salmi, *Chem. Eng. J.* **2012**, *207–208*, 539–551. DOI: https://doi.org/10.1016/j.cej.2012.07.015

[31] D. Bothe, A. Reusken, *Transport Processes at Fluidic Interfaces*, Springer International Publishing, Cham **2017**.

[32] H. E. H. Meijer, M. K. Singh, P. D. Anderson, *Progress Polym. Sci.* **2012**, *37 (10)*, 1333–1349. DOI: https://doi.org/10.1016/j.progpolymsci.2011.12.004

[33] R. K. Rahmani, T. G. Keith, A. Ayasoufi, *J. Heat Transfer* **2006**, *128 (8)*, 769–783. DOI: https://doi.org/10.1115/1.2217749

[34] L. L. Trinkies, B. J. Deschner, E. Hansjosten, M. Kraut, R. Dittmeyer, *Chem. Ing. Tech.* **2020**, *92 (9)*, 1364. DOI: 10.1002/cite.202055312

Spatially Resolved Simulation of Fluid Flow During Direct Synthesis of H_2O_2 in a Microstructured Membrane Reactor

L. L. Trinkies*, A. Düll, B. J. Deschner, A. Stroh, M. Kraut, R. Dittmeyer

Communication: A CFD model of a microstructured membrane reactor with integrated fluid guiding elements for the direct synthesis of hydrogen peroxide is developed and implemented in the form of a customized solver in OpenFOAM®. To optimize the process window of the operational and design parameters, the impact of the insert's geometry on the reactor's performance is investigated. .... ■